

Data-driven effective model shows a liquid-like deep learning

Wenxuan Zou and Haiping Huang*

PMI Lab, School of Physics, Sun Yat-sen University, Guangzhou 510275, People's Republic of China

(Dated: December 10, 2021)

Geometric structure of an optimization landscape is argued to be fundamentally important to support the success of deep learning. However, recent research efforts focused on either of toy random models with unrealistic assumptions and numerical evidences about different shapes of the optimization landscape, thereby lacking a unified view about the nature of the landscape. Here, we propose a statistical mechanics framework by directly building a least structured model of the high-dimensional weight space, considering realistic structured data, stochastic gradient descent algorithms, and the computational depth of the network parametrized by weight parameters. We also consider whether the number of network parameters outnumbers the number of supplied training data, namely, over- or under-parametrization. Our least structured model predicts that the weight spaces of the under-parametrization and over-parameterization cases belong to the same class. These weight spaces are well-connected without any heterogeneous geometric properties. In contrast, the shallow-network has a shattered weight space, characterized by discontinuous phase transitions in physics, thereby clarifying roles of depth in deep learning. Our effective model also predicts that inside a deep network, there exists a liquid-like central part of the architecture in the sense that the weights in this part behave as randomly as possible. Our work may thus explain why deep learning is unreasonably effective in terms of the high-dimensional weight space, and how deep networks are different from shallow ones.

I. INTRODUCTION

Artificial deep neural networks have achieved the state-of-the-art performances in many industrial and academic domains ranging from pattern recognition and natural language processing [1] to many-body quantum physics and classical statistical physics [2]. However, it remains challenging to reveal mechanisms underlying the success of deep learning. One key obstacle is building the causal relationship between the high-dimensional non-convex optimization landscape and the state-of-the-art performances of deep networks [3]. In past few years, many theoretical and empirical efforts contributed to understanding this fundamental relationship. Poor local minima of the optimization landscape are rare in the over-parametrization regime where the number of trainable parameters (weights) in a typical deep network is much larger than the number of training data [4]. All minima in the landscape were shown to be global minima, given special requirements for network architectures and neural activation functions [5]. In particular, no substantial barriers between minima are observed in deep learning [6]. Even these minima can be connected via hyperpaths within a unique global valley [7–9]. The geometric structure of local minima was also extensively studied [10–12]. Among these studies, the concept of flat minima is attractive yet remains controversial [13–16]. The flat minima implies that the weights around them can be perturbed without significantly changing the training cost function. The flatness of such minima was empirically supported by the eigen-spectrum of the Hessian matrix evaluated at those minima [11]. The curvature of the landscape was also claimed to correlate with the generalization ability of deep networks for unseen data [17]. Therefore, studying deep networks from the perspective of the high-dimensional weight space is a hot topic yet under heated debate.

Physics methods have been applied to investigate the weight space structure of non-convex high-dimensional problems, e.g., the spherical/binary spin model approximation of deep neural networks [18–21], and the weight space structure of binary perceptron problems [22–24]. However, one drawback of these studies lies at their strong assumptions to build toy models. These models assume unstructured data as well as shallow networks, and moreover the learning behavior is far from the practical training procedure used in a typical deep learning. Therefore, the community has not reached conclusive analytic results about what the geometric structure of the deep-learning landscape looks like.

Here, from a conceptually different viewpoint, we propose a data-driven effective model, taking into account interactions among structured data, deep architectures, and training. We consider deep networks of binary weights that are amenable for theoretical analysis and moreover can be efficiently trained with mean-field methods [25]. Then the weight configurations realizing a high classification accuracy of the structured data are collected as a large ensemble,

*Electronic address: huanghp7@mail.sysu.edu.cn

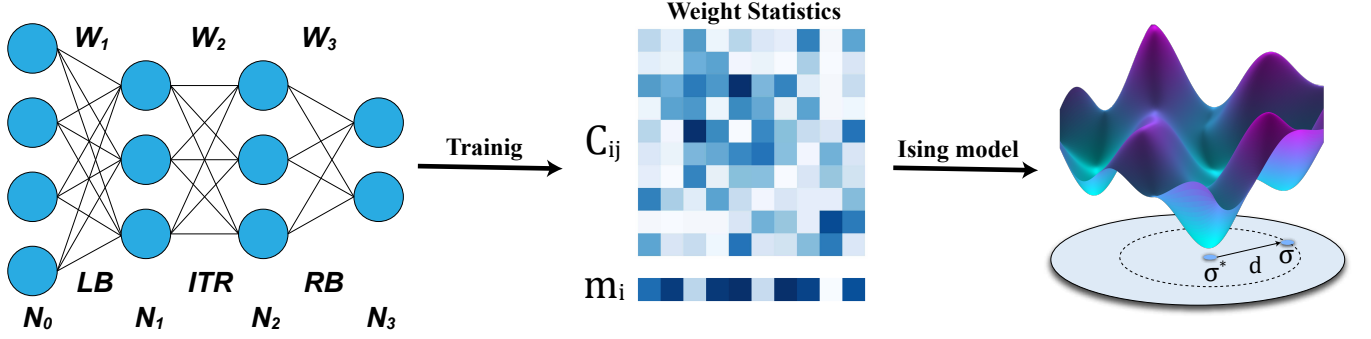


FIG. 1: Schematic illustration of how to construct an effective physics model analyzing the deep-learning weight space. We consider a four-layer neural network of binary weights to perform a classification task, where the input data pass through the weight regions of the left boundary (LB), the interior (ITR), and the right boundary (RB) in order. After the neural network is trained from different initializations, the weight statistics including magnetizations (first-order moments) $m_i = \langle \sigma_i \rangle$ and pairwise correlations (second-order moments) $C_{ij} = \langle \sigma_i \sigma_j \rangle$ will be computed directly from the collected weight configurations. Based on the weight statistics, we establish an effective data-driven Ising model that is able to reflect the weight space characteristics, and then apply the entropy landscape analysis by introducing a distance-dependent extra term into the Boltzmann distribution of the effective Ising model. The entropy landscape analysis can help to explore the internal structure of the weight parameter space by counting how dense weight parameters σ are at a typical distance d away from the reference one σ^* .

whose statistics is described by first-order and second-order moments. The maximum-entropy principle [26] then applies to construct a minimal model of the weight space. The maximum-entropy principle is also a powerful tool to analyze neural population at the collective network-activity level [27, 28]. This effective model of the practical deep learning is then analyzed from a statistical mechanics perspective, in which the geometric structure of the entire weight space can be characterized in different contexts: over-parametrization, under-parametrization and shallow networks. Many intriguing properties of the geometric structure can thus be revealed, providing a coherent picture about the landscape. Most interestingly, the results claim that deep learning shapes a large liquid-like core in the weight space for the central part of the architecture, pointing towards a general principle underlying the success of deep learning, in consistent with other studies from different angles [29, 30].

II. DEEP LEARNING SETTING

In order to collect weight configurations in the neural network parameter space, we design a neural network architecture to solve the classification task of the handwritten digits (or the MNIST dataset [31]) first, and then an extensive number of weight solutions that lead to high test accuracy are collected. The test accuracy refers to the network's ability to classify unseen dataset. More precisely, we consider a four-layer fully-connected feedforward network. Each layer has N_l ($l = 0, 1, 2, 3$) neurons, where N_0 equals to the dimension of the input vector, and N_3 equals to the number of total classes. The weight matrix W^l indicates connections between layer l and layer $l - 1$ (Fig. 1). For simplicity, we do not consider biases for neurons. The neural activity (including the input) is transferred by a non-linear function, i.e., the leaky ReLU (L-ReLU) function defined by $\max(0, z) + 0.1 \min(0, z)$, where z denotes the pre-activation or the weighted-sum of input activities. We finally add a softmax layer after the output layer and use the cross entropy as the loss function.

To collect a sufficient number of weight configurations and facilitate theoretical analysis, we require that the neural network architecture should meet two demands. First, the model complexity, namely, the number of the total weights should be small. This avoids a sharp growth of the computational cost consumed to collect a huge number of weight configurations. Second, the weight of the neural network should take binary values $\{+1, -1\}$, as the following analyses are based on the Ising model, in which the weights are analogous to the spins in a physics model.

To fulfill the first demand, we should first create a set of input data with low dimension. Thus, we carry out a principal component analysis (PCA) of the MNIST dataset, retaining only the top 20 principal components, which explain about 64.5% of the total variance in the original data. After this dimension reduction, a relatively high-quality reconstruction of the digits can be performed. Although the loss of information will degrade the test accuracy, we can still reach a relatively high test accuracy (see Appendix C).

Because of the second demand, the network with binary weights is difficult to train by the standard gradient decent algorithm, due to the fact that the cost function is not differentiable with respect to the discrete synaptic weight. To

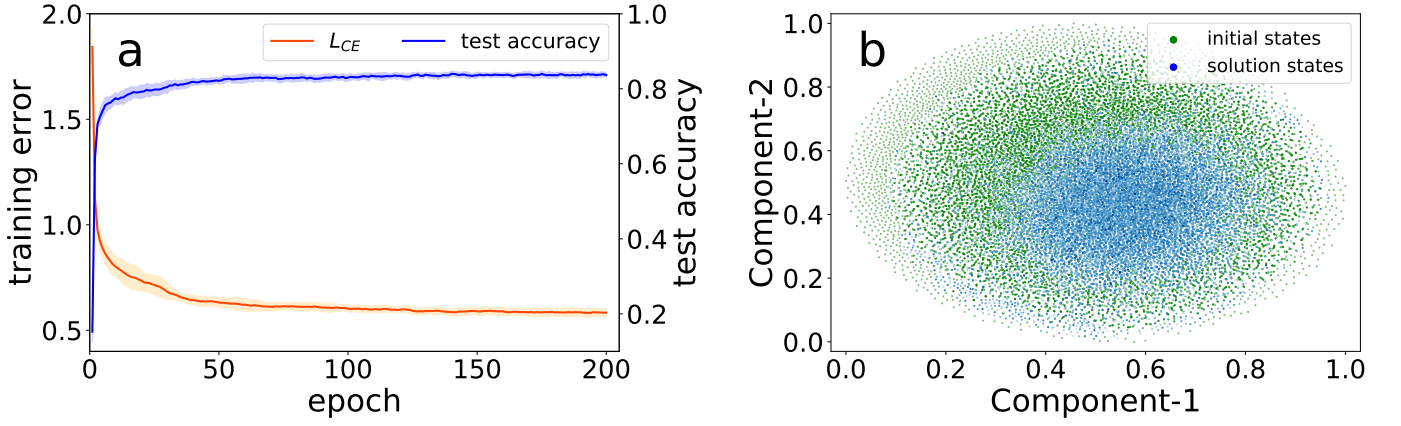


FIG. 2: Neural network training and properties of weight configurations sampled from independent runs of training. (a) Training trajectories of four-layer networks. The cross-entropy (the orange line) and test accuracy (the blue line) can reach 0.2 and 85%, respectively at the 200-th epoch, where the fluctuation indicated by the shadow regime is computed from ten independent training runs. (b) Two-dimensional representations of 20 000 random initializations (green dots) and 20 000 learned weight configurations (blue dots). The low dimensional projection is carried out by the t-SNE technique [33]. The random initialization denotes the weight configuration (or state) sampled by the Gaussian random initial fields θ_0 . The collected weight configurations (or solution states) are obtained at the end of the training starting from the initial fields θ_0 . For the solution states, the deeper their colors are, the higher the corresponding test accuracies are, while the random initial states are all of the same green color of chance-level accuracy.

tackle this challenge, we apply a recently-proposed mean-field training algorithm [25]. More precisely, we consider the situation that each weight w_{ij}^l follows a binomial distribution $P(w_{ij}^l)$ parametrized by an external field θ_{ij}^l as follows:

$$P(w_{ij}^l) = \sigma(\theta_{ij}^l) \delta_{w_{ij}^l, 1} + [1 - \sigma(\theta_{ij}^l)] \delta_{w_{ij}^l, -1}, \quad (1)$$

where $\sigma(\cdot)$ is a sigmoid function. The external fields are clearly continuous. Therefore, the standard backpropagation can be applied to the external fields $\{\theta_{ij}^l\}$, instead of weights (ill-defined in gradients).

In the feedforward transformation, the pre-activation can be written as $z_j^l = \sum_i w_{ij}^l a_i^{l-1}$, where a_i^{l-1} is the activation at the layer $l-1$. The weight w_{ij}^l is subject to the aforementioned binomial distribution, and thus its mean and variance, i.e., μ_{ij}^l and $(\sigma_{ij}^l)^2$, are given by:

$$\mu_{ij}^l = \langle w_{ij}^l \rangle = 2\sigma(\theta_{ij}^l) - 1, \quad (2a)$$

$$(\sigma_{ij}^l)^2 = \langle (w_{ij}^l)^2 \rangle - \langle w_{ij}^l \rangle^2 = -4\sigma^2(\theta_{ij}^l) + 4\sigma(\theta_{ij}^l). \quad (2b)$$

To avoid a direct sampling process, we use the local re-parametrization trick [32]. According to the central limit theorem, z_j^l can then be approximated to follow a Gaussian distribution $z_j^l \sim \mathcal{N}(\sum_i \mu_{ij}^l a_i^{l-1}, \sum_i (\sigma_{ij}^l)^2 (a_i^{l-1})^2)$. Hereafter, we define the mean and variance of z_j^l to be m_j^l and $(v_j^l)^2$, respectively. Taken together, the feedforward transformation can be finally re-parametrized as:

$$z_j^l = m_j^l + v_j^l \cdot \epsilon_j^l, \quad (3a)$$

$$a_j^l = \frac{1}{\sqrt{N_{l-1}}} \text{L-ReLU}(z_j^l), \quad (3b)$$

where ϵ_j^l is a standard Gaussian random variable, and $\frac{1}{\sqrt{N_{l-1}}}$ is a scaling factor to eliminate the layer-width dependence of the activation a_j^l . Detailed training procedures are given to Appendix A.

In practice, we use two hidden layers with 15 neurons for each. The widths of input layer and output layer are determined by the data, which are 20 and 10, respectively. Thus, our network architecture is specified by 20-15-15-10, resulting in the number of weight parameters $N = 675$. Unless stated otherwise, we use the entire MNIST dataset (i.e., 60 000 digits examples) for training and the other 10 000 examples for testing. By fine tuning hyper-parameters of the training procedure (see Appendix C), the neural network can reach a test accuracy of 85% [Fig. 2(a)], i.e., the trained network can classify correctly 85% of the unseen test dataset. To collect distinct weight configurations, we

train the neural network for 50 epochs starting from a random Gaussian initialization of external fields θ during each sampling trial. Then, we use the trained external fields to generate 10 weight configurations and select the one with the optimal test accuracy ($\geq 80\%$). In this way, we obtain two million weight configurations with test accuracies ranged from 80% to 83%, for constructing an effective model.

To give a brief picture of the weight parameter space, we apply the t-SNE dimension reduction technique [33] to 20 000 random initialization points and the corresponding learned weight configurations with the same number. Here, random initialization points represent the weight parameters sampled from the Gaussian-initialized external fields, from which the external fields are trained to reach the test accuracy threshold. The collected weight configurations are sampled from the final binomial distribution. Note that the dominant part of the weight configuration space (valid weights realizing the classification task) seems to be organized into a large connected component [Fig. 2 (b)], which also indicates that compared to the entire parameter space, the weight space realizing the classification task occupies a relatively small region. Next, we design a semi-rigorous statistical mechanics framework to explore a detailed high-dimensional geometric structure of the weight space for the current deep-learning model.

III. DATA-DRIVEN ISING MODEL

We build a data-driven Ising model to describe the two million weight configurations, as we are interested in the statistical properties of the deep-learning weight space. More precisely, weight parameter solutions $\mathbf{W} = \{w_1, w_2, \dots, w_N\}$ are transformed to spin configurations $\sigma = \{\sigma_1, \dots, \sigma_N\}$ in the following analysis. Given the constraints of weight statistics including magnetization (first-order moments) $m_i = \langle \sigma_i \rangle$ and pairwise correlation (second-order moments) $C_{ij} = \langle \sigma_i \sigma_j \rangle$, the least-structured-model probability distribution $P(\sigma)$ to fit the weight statistics follows the maximum entropy principle [26] (see also Fig. 1 for an illustration). According to this principle, $P(\sigma)$ is recast into the form of the Boltzmann distribution:

$$P(\sigma) = \frac{1}{Z} \exp(-\beta E(\sigma)), \quad (4)$$

where Z is the partition function in statistical physics, β is the inverse temperature ($\beta = 1$ throughout the paper as it can be absorbed into the model parameters), and $E(\sigma) = -\sum_{i<j} J_{ij} \sigma_i \sigma_j - \sum_i h_i \sigma_i$ is the energy that is consistent with the Ising-model's Hamiltonian. The model parameter J_{ij} denotes the functional coupling between weight σ_i and weight σ_j interpreting the second-order correlation among weights, where $J_{ij} > 0$ and $J_{ij} < 0$ refer to ferromagnetic and anti-ferromagnetic interactions, respectively. The model parameter h_i denotes the bias of the weight σ_i , reflected by the external field on the weight σ_i after training.

To find the model parameters $\Omega = \{\mathbf{J}, \mathbf{h}\}$, we use the gradient accent algorithm corresponding to the maximum likelihood learning principle. By maximizing the log-likelihood $\langle \ln(P_{\Omega}(\sigma)) \rangle_{\text{weight-data}}$ with respect to the model parameters $\Omega = \{\mathbf{J}, \mathbf{h}\}$, we can obtain the following iterative learning rules [34]:

$$J_{ij}^{t+1} = J_{ij}^t + \eta (\langle \sigma_i \sigma_j \rangle_{\text{data}} - \langle \sigma_i \sigma_j \rangle_{\text{model}}), \quad (5a)$$

$$h_i^{t+1} = h_i^t + \eta (\langle \sigma_i \rangle_{\text{data}} - \langle \sigma_i \rangle_{\text{model}}), \quad (5b)$$

where t and η denote the learning step and learning rate, respectively. In the above learning equation, the data expectation terms can be directly computed from the sampled parameter solutions. However, the model expectation terms are commonly difficult to compute due to the $\mathcal{O}(2^N)$ computation complexity. Fortunately, the cavity method in spin glass theory (Appendix B) can be used to approximate the model expectations. At each learning step, to evaluate how well the Ising model fits the weight statistics, we compute the root-mean squared error (or deviation) between the data expectations and model expectations:

$$\Delta = \sqrt{\frac{1}{N} \sum_i [m_i^{\text{data}} - m_i^{\text{model}}]^2 + \frac{2}{N(N-1)} \sum_{i<j} [C_{ij}^{\text{data}} - C_{ij}^{\text{model}}]^2}, \quad (6)$$

from which a perfect fitting leads to a zero deviation. We stop the learning when $\Delta < 0.01$ or after 300 learning steps are reached.

In Fig. 3(b), we verify that the reconstructed magnetizations and correlations from the data-driven Ising model are in good agreement with the measured ones, which ensures that the data-driven Ising model is an effective model whose model parameters $\Omega = \{\mathbf{J}, \mathbf{h}\}$ capture statistical properties of the deep-learning weight space. The histogram of the model parameters is shown in Fig. 3(a). Note that most of the couplings are concentrated around zero value for the full model, despite a relatively less frequent tail. In contrast, the bias is broadly distributed. To get more insights about the model parameters, we plot the histogram for different sub-parts of the deep network [Fig. 3(d)]. Compared

to the boundaries, i.e., LB and RB, the interior's couplings are more concentrated around zero value, and moreover the corresponding biases are all concentrated around 0.25 corresponding to the highest peak in the histogram of Fig. 3 (a), which clearly implies that weights in the interior of the deep network have weak correlations, behaving like in a high temperature phase, as we shall prove semi-rigorously. More precisely, 20 peaks in the LB's bias distribution correspond to 20 input neurons, while 10 peaks in the RB's bias distribution correspond to 10 output neurons.

Given the model parameters of the constructed Ising model, we can compute the model energy of every weight configuration directly. Fig. 3(c) shows the model energy density versus the test accuracy. Though the fluctuation is large, we find that low energy configurations tend to have high accuracies, which helps to build an intuitive relationship between the model energy landscape and the deep-learning landscape.

IV. ENTROPY LANDSCAPE ANALYSIS

In the previous section, we construct an effective Ising model, whose model parameters preserve the information up to second order correlations of the weight space. In order to explore the internal structure of the weight space of the deep learning, we introduce a distance-dependent term $x \sum_i \sigma_i^* \sigma_i$ in the original Boltzmann distribution [Eq. (4)] as follows [28]:

$$P(\boldsymbol{\sigma}) = \frac{1}{Z} \exp \left(\beta \sum_{i < j} J_{ij} \sigma_i \sigma_j + \beta \sum_i h_i \sigma_i + x \sum_i \sigma_i^* \sigma_i \right), \quad (7)$$

where $\boldsymbol{\sigma}^*$ is the reference weight configuration, and x is the coupling field constraining the distance between the configuration $\boldsymbol{\sigma}$ and the reference one $\boldsymbol{\sigma}^*$. Intuitively, $x > 0$ implies that the weight configurations closer to the reference are preferred, while $x < 0$ implies that the weight configuration far away from the reference are preferred (see Fig. 1 for an illustration).

Then the geometric structure of the high-dimensional weight space can be summarized into the constrained free energy function given below.

$$\beta f \equiv -\frac{1}{N} \ln \sum_{\boldsymbol{\sigma}} \exp \left(-\beta E(\boldsymbol{\sigma}) + x \sum_i \sigma_i^* \sigma_i \right), \quad (8)$$

where $E(\boldsymbol{\sigma})$ is the Hamiltonian of the effective model. We further introduce the energy density $\epsilon = E(\boldsymbol{\sigma})/N$ and the overlap $q = \sum_i \sigma_i \sigma_i^*/N$. It then follows that

$$\begin{aligned} \beta f &= -\frac{1}{N} \ln \iint d\epsilon dq \exp \left(-N\beta\epsilon + Nxq + \ln \sum_{\boldsymbol{\sigma}} \delta \left(\epsilon - \frac{E(\boldsymbol{\sigma})}{N} \right) \delta \left(q - \frac{\sum_i \sigma_i \sigma_i^*}{N} \right) \right) \\ &= -\frac{1}{N} \ln \iint d\epsilon dq \exp (-N\beta f(\epsilon, q)), \end{aligned} \quad (9)$$

where $\beta f(\epsilon, q) \equiv \beta\epsilon - xq - s(\epsilon, q)$ is the constrained free energy as a function of energy density ϵ and overlap q . This constrained free energy captures the competition between the model energy and entropy. The entropy is defined by $s(\epsilon, q) = 1/N \ln \sum_{\boldsymbol{\sigma}} \delta(\epsilon - \frac{E(\boldsymbol{\sigma})}{N}) \delta(q - \frac{\sum_i \sigma_i \sigma_i^*}{N})$, measuring the log-number of the weight configurations with energy $N\epsilon$ and overlap q given a reference.

When the system size N (675 in this paper) is large in Eq. (9), the Laplace method can be used to approximate the integral by taking only the dominant contribution. Hence, $f \approx \min_{\epsilon, q} f(\epsilon, q)$. To estimate the minimal free energy density $f(\epsilon, q)$ and the corresponding saddle-point values (ϵ, q) , we iteratively solve the mean-field equations based on the cavity approximation (Appendix B). Then, the entropy density $s(\epsilon, q)$ is calculated via the double Legendre transformation $s(\epsilon, q) = -\beta f + \beta\epsilon - xq$. For the convenience in the further analyses, we introduce the Hamming distance $(N - \sum_i \sigma_i \sigma_i^*)/2$, which counts the number of weights that are distinct between the target configuration $\boldsymbol{\sigma}$ and the reference one $\boldsymbol{\sigma}^*$. The Hamming distance per weight d can thus be transformed from the overlap by $d = (1 - q)/2$. In the following analysis, we omit the energy density dependence of $s(\epsilon, q)$ and write it as the function of d , i.e., $s(d)$. We also assume $\beta = 1$, as the inverse temperature has been absorbed into the inferred couplings and biases of the effective model (see Sec. III).

To have a complete understanding of the deep-learning landscape, we analyze three representative scenarios. The first one is the under-parametrization case, in which the number of training examples is larger than the network-parameter size N . The second one is the over-parametrization case where the number of training examples is smaller than the network-parameter size N , and the last one is the shallow-network case where all hidden layers are deleted (for more details, see the Appendix C).

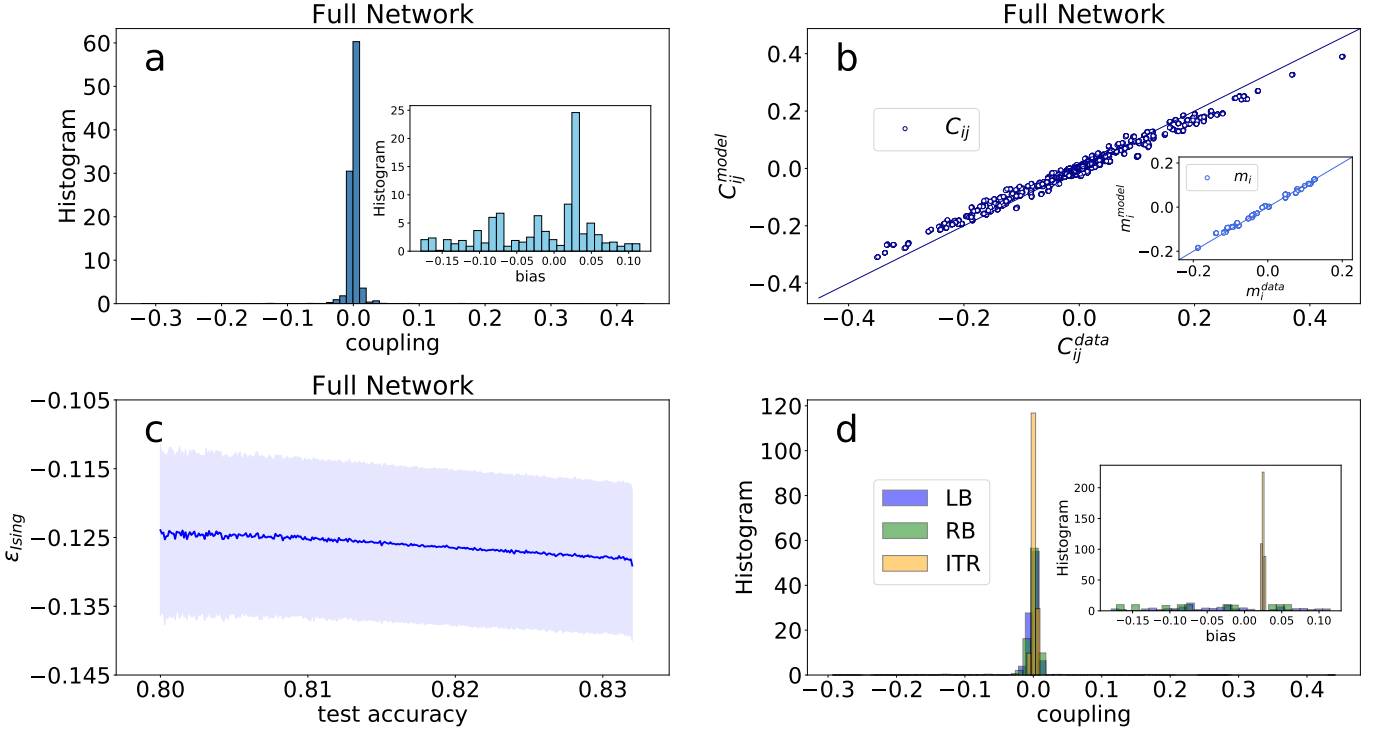


FIG. 3: Properties of the data-driven Ising model. (a) Histograms of full-model (all) parameters. Couplings J_{ij} and biases h_i (inset) are shown. (b) Reconstructed correlation C_{ij} and magnetization m_i (inset) from the effective Ising model versus the measured ones for the full model. Full lines indicate the equality. (c) Ising energy density ϵ_{Ising} versus test accuracy of the full model. Each accuracy corresponds to a large amount of weight configurations, where the blue line indicates expectation values and the light blue shadow denotes the fluctuation. (d) Histograms of model parameters in sub-parts (see Fig. 1) of the deep hierarchy. Couplings J_{ij} and biases h_i (inset) are shown.

A. Under-parametrization scenario

In the under-parametrization case, the number of supplied training examples is much larger than the network-parameter size (or the model complexity). As expected, we do not find any weight-space-structure induced phase transitions, unlike in a similar study in neural coding space [28]. First, the distance d increases or decreases continuously following either of two directions of changing the coupling field [Fig. 4 (a)]; both directions collapse into a single curve, without any hysteresis phenomenon. This provides a strong evidence that the weight space is connected in the absence of thermodynamically-dominant barriers. This result of the effective model coincides roughly with the low-dimensional projection evidence shown in Fig. 2 (b) as well.

Let us then look at the entropy landscape. The entropy landscape is also smooth. For a system with discrete degrees of freedom, one can easily compute the upper bound for the entropy $s_{ub}(d) = -d \ln d - (1 - d) \ln(1 - d)$ with the unique constraint of the distance between any two weight configurations in the high-dimensional space. One salient feature is that three sub-parts of the deep architecture display distinct behaviors, despite a common smooth landscape. Surprisingly, the interior region shows an entropy nearly saturating the upper bound. This region in physics behaves like a liquid state, where there exist many realizations of weights to fulfill the classification task of the deep network, and the learning dynamics is thus fast in this region. However, the right or left boundaries are more constrained than the interior region with lower entropy values. The left boundary is the most constrained one among all three parts of the deep network, while the right boundary behaves similarly to the full network of three parts. An intuitive interpretation is that, two boundaries are directly responsible for encoding or decoding the input-output relationship embedded in the training dataset. Allowing more freedoms in these two boundaries will sacrifice the generalization capability of the network, which is also evidenced in our recent work of learning credit assignments [30]. In sum, the under-parametrization does not lead to a shattered weight space, with a liquid-like interior next to two more constrained boundaries.

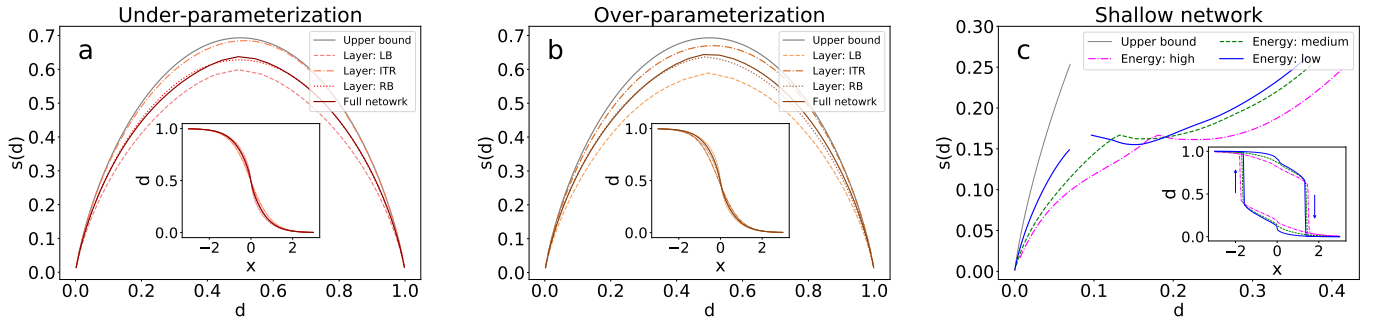


FIG. 4: Entropy landscape analyses in three different scenarios of deep learning. (a) Under-parametrization case. The curves are the mean results over 20 distinct reference weight configurations σ^* selected from the low energy region (for references coming from high- and medium-energy regions, see Fig. 5 and Fig. 6 in Appendix C). Entropy curves are plotted along the direction of the decreasing coupling field x from 3 to -3 , while the Hamming distance per weight d versus x is plotted by considering two directions of increasing and decreasing x (inset). No hysteresis loops and entropy gaps are observed. (b) Over-parametrization case. Other conditions are the same as (a). (c) Shallow network case. The inset shows a hysteresis loop for distance d versus coupling field x , and the entropy curves correspond to the lower-branch of the hysteresis loop. A first-order phase transition arises in this case showing a complex landscape in the high-dimensional weight space.

B. Over-parametrization scenario

We then ask whether the nice property of the under-parametrization case transfers to the over-parametrization case, which is the popular setting in the current deep learning era. We thus investigate the over-parametrization case, where the number of training examples is less than the model complexity (Appendix C). We surprisingly find that the qualitative properties of the under-parametrization case also hold in the over-parametrization case [Fig. 4 (b)], in an excellent agreement with recent empirical studies of deep learning at a large-scale architecture [6–8]. However, we notice a salient difference that the extent the interior entropy gets close to the upper bound is weaker than that of the under-parametrization case, despite the fact that the interior entropy is still highest among three parts of the deep network. Even in the over-parametrization case, a liquid-like interior inside the network exists, coinciding exactly with a recent study of deep networks in both random inputs/outputs setting and teacher-student generalization setting [29]. This recent study claimed a glass-liquid-glass/solid-liquid-solid pattern inside the deep-learning architecture. Despite a relatively small scale for the sake of the data-driven analytical study, our work claims the same phenomenon in the central part of the deep network by constructing an effective data-driven model for a practical deep learning. Although we do not observe a glass/solid like boundaries (unlike in the recent study [29]), these two boundaries are clearly more constrained than the central part. We thus expect that these boundaries may enter a glass/solid phase in the thermodynamic limit, which is a very interesting future direction.

C. Shallow networks

To explore the benefit of depth, an important characteristic of the deep learning, we study a shallow-network architecture without any hidden layers. Other conditions are the same with the other two scenarios. Using the same statistical mechanics framework, we surprisingly find a first-order phase transition in the distance-coupling-field profile [Fig. 4 (c)]. The discontinuous transition is characterized by a hysteresis loop and associated entropy gaps, irrespective of references selected from high-, medium- and low-energy regions. For the shallow-network case, the weight space is shattered into clusters separated by entropy gaps. In particular, a double-discontinuous transition is even observed for the low-energy references, implying that the weight space around the low-energy references becomes much more complex, as also revealed in a biological data analysis of retina coding [28].

Compared to the deep network, the dynamics in the shallow network can be strongly affected by the discontinuous transition because of metastability in thermodynamic states. When adding more hidden layers, the shattered weight space is replaced by a connected smooth sub-space, demonstrating the benefit of depth. Our effective model thus provides a theoretical tool to distinguish a shallow network from a deep one.

V. CONCLUSION

Previous studies along the line of exploring the weight-space landscape of deep learning focused on either non-practical toy models [4, 18–20, 29] or empirical studies of practical deep training [11, 12, 14, 15, 35]. In contrast, we build a data-driven effective model to describe the geometric structure of the deep-learning weight space. The weight data to establish the effective model comes from a practical training; only up to the second order correlation in the weight space is considered for simplicity.

Our effective model reveals several interesting phenomena. First, the model can distinguish a deep network from a shallow one in terms of weight-space geometric structure. The deep network weight-space is smooth and dominated by a connected component, while a shattered weight space emerges in the shallow network, displaying a discontinuous transition in the Hamming distance profile. Second, for the deep network, the under-parametrization and over-parametrization belong to the same class, in the sense that their weight spaces are identically dominated by a single connected component, which is consistent with recent empirical studies that claimed no substantial barriers between minima in the deep-learning loss landscape [6–8]. Our analysis may thus support the success of deep learning despite the NP-hardness (worst case) of the deep learning problem. A recent work revealed that as the model complexity of continuous weights increases, the generalization error displays a cusp around a critical value of the complexity; on both sides of this cusp, the generalization error decays [36]. It is thus interesting in future works to see whether there exists a qualitative change in the geometric structure of the weight space around the cusp. Third, a special interior part of a largest entropy in the weight space exists, showing a liquid-like property. In the under-parametrization case, this giant interior landscape even gets very close to the upper bound of completely random space. The existence of the liquid-like central part coincides exactly with two recent studies: one is the toy random models of deep learning [29], as discussed in Sec. IV B; the other is the ensemble backpropagation applied to practical deep learning [30], which found a peak of model entropy in the central part of the deep network.

Our work demonstrates that the statistical physics framework is a promising tool to draw a complete geometric picture of the deep-learning landscape, and thus paves the way towards understanding the conflict between the effectiveness of deep learning and the training failures predicted by traditional statistical learning theory.

Acknowledgments

We would like to thank other members of PMI lab for a long-term discussion of this project. This research was supported by the National Key R&D Program of China (2019YFA0706302), the start-up budget 74130-18831109 of the 100-talent- program of Sun Yat-sen University, and the NSFC (Grant No. 11805284).

Appendix A: Mean-field training algorithms

To train a deep supervised network with binary weights, we apply the mean-field method first introduced in the previous work [25]. In our current setting, each weight w_{ij}^l is sampled from a binomial distribution $P(w_{ij}^l)$ parametrized by an external field θ_{ij}^l as follows,

$$P(w_{ij}^l) = \sigma(\theta_{ij}^l) \delta_{w_{ij}^l, 1} + [1 - \sigma(\theta_{ij}^l)] \delta_{w_{ij}^l, -1}, \quad (\text{A1})$$

with mean $\mu_{ij}^l = 2\sigma(\theta_{ij}^l) - 1$ and variance $(\sigma_{ij}^l)^2 = -4\sigma^2(\theta_{ij}^l) + 4\sigma(\theta_{ij}^l)$. According to the central-limit theorem, the feedforward transformation can be re-parametrized as:

$$z_j^l = m_j^l + v_j^l \cdot \epsilon_j^l, \quad (\text{A2a})$$

$$a_j^l = \frac{1}{\sqrt{N_{l-1}}} \text{L-ReLU}(z_j^l), \quad (\text{A2b})$$

where $m_j^l = \sum_i \mu_{ij}^l a_i^{l-1}$, and $v_j^l = \sqrt{\sum_i (\sigma_{ij}^l)^2 (a_i^{l-1})^2}$.

During the error backpropagation phase, we need to compute the gradient of the loss function \mathcal{L} [e.g., L_{CE} in Fig. 2 (a)] with respect to the external field θ , which proceeds as follows:

$$\frac{\partial \mathcal{L}}{\partial \theta_{ij}^l} = \frac{\partial \mathcal{L}}{\partial z_j^l} \frac{\partial z_j^l}{\partial \theta_{ij}^l} = \frac{\partial \mathcal{L}}{\partial z_j^l} \left(\frac{\partial m_j^l}{\partial \theta_{ij}^l} + \epsilon_j^l \frac{\partial v_j^l}{\partial \theta_{ij}^l} \right). \quad (\text{A3})$$

We then define $\Delta_j^l \equiv \frac{\partial \mathcal{L}}{\partial z_j^l}$. On the top layer, $\Delta_j^l = y_j^L - \hat{y}_j^L$, where $y_j^L = \frac{e^{z_j^L}}{\sum_i e^{z_i^L}}$ is the softmax output, and \hat{y}_j^L is the (one-hot) label of the input. On the lower layers, given Δ_k^{l+1} , we can iteratively compute Δ_j^l :

$$\begin{aligned} \frac{\partial \mathcal{L}}{\partial z_j^l} &= \sum_k \frac{\partial \mathcal{L}}{\partial z_k^{l+1}} \frac{\partial z_k^{l+1}}{\partial z_j^l} \\ &= \sum_k \Delta_k^{l+1} f'(z_j^l) \left(\mu_{jk}^{l+1} + \epsilon_k^{l+1} \frac{(\sigma_{ij}^l)^2 a_j^l}{v_k^{l+1}} \right). \end{aligned} \quad (\text{A4})$$

Finally, we compute $\frac{\partial m_j^l}{\partial \theta_{ij}^l}$ and $\frac{\partial v_j^l}{\partial \theta_{ij}^l}$, respectively. It then proceeds as follows.

$$\frac{\partial m_j^l}{\partial \theta_{ij}^l} = \frac{\partial m_j^l}{\partial \mu_{ij}^l} \frac{\partial \mu_{ij}^l}{\partial \theta_{ij}^l} = 2a_i^{l-1} \sigma'(\theta_{ij}^l), \quad (\text{A5a})$$

$$\frac{\partial v_j^l}{\partial \theta_{ij}^l} = \frac{\partial v_j^l}{\partial (\sigma_{ij}^l)^2} \frac{\partial (\sigma_{ij}^l)^2}{\partial \theta_{ij}^l} = -2 \frac{(a_i^{l-1})^2 \mu_{ij}^l \sigma'(\theta_{ij}^l)}{v_j^l}. \quad (\text{A5b})$$

Note that ϵ is sampled and quenched for both forward and backward computations in a single mini-batch gradient descent. After the learning is terminated, an effective network with binary weights can be constructed by sampling the binomial distribution parametrized by external fields.

Appendix B: Cavity method for landscape analysis

To analyze the statistical properties of the least structured model, we apply the cavity method in the spin glass theory [37]. Note that the weight configuration follows the Boltzmann distribution $P(\boldsymbol{\sigma}) = \exp(-\beta E(\boldsymbol{\sigma})) / Z$, where the energy $E(\boldsymbol{\sigma}) = -\sum_{i < j} J_{ij} \sigma_i \sigma_j - \sum_i h_i \sigma_i$, and Z is the partition function. An exact computation of the free energy $(-T \ln Z)$ is an NP-hard problem. To get an approximate free energy, we first compute the free energy change ΔF_i when adding a weight (e.g., σ_i) and its associated interactions. We then calculate the free energy change ΔF_a when adding an interaction (e.g., $J_a \sigma_i \sigma_j$, and $a \equiv (ij)$). In all these derivations, we make an assumption that when an interaction is removed, its neighboring weights become independent such that the joint distribution of them becomes factorized, which is exact if the factor graph of the model is locally tree-like. The factor graph is a bipartite graph where two kinds of nodes (weight nodes and interaction nodes) are present. For detailed derivations, interested readers are recommended to go through the standard textbook [38], or the appendix of a recent paper [39]. In the cavity approximation, the free energy can be constructed as below,

$$F \equiv -\frac{1}{\beta} \ln Z = \sum_i \Delta F_i - \sum_a (|\partial a| - 1) \Delta F_a, \quad (\text{B1a})$$

$$\beta \Delta F_i = -\ln \sum_{x=\pm 1} \mathcal{H}_i(x), \quad (\text{B1b})$$

$$\mathcal{H}_i(x) \equiv e^{x\beta h_i} \prod_{b \in \partial i} \cosh \beta J_b (1 + x \hat{m}_{b \rightarrow i}), \quad (\text{B1c})$$

$$\beta \Delta F_a = -\ln \cosh \beta J_a - \ln \left(1 + \tanh \beta J_a \prod_{i \in \partial a} m_{i \rightarrow a} \right), \quad (\text{B1d})$$

where $|\partial a|$ denotes the number of weights connected to the interaction a , $i \in \partial a$ denotes the neighboring weights i of the interaction a , and $a \in \partial i$ denotes the neighboring interactions a of the weight i . $m_{j \rightarrow b}$ is the cavity magnetization of weight j in the absence of the interaction a , and $\hat{m}_{b \rightarrow i} = \tanh \beta J_b \prod_{j \in \partial b \setminus i} m_{j \rightarrow b}$ is the conjugate magnetization.

According to the variational principle, the free energy should be stationary with respect to $\{m_{i \rightarrow a}\}$. We can then obtain a set of self-consistent equations called message passing equations as follows,

$$m_{i \rightarrow a} = \tanh \left(\beta h_i + \sum_{b \in \partial i \setminus a} \tanh^{-1} \hat{m}_{b \rightarrow i} \right), \quad (\text{B2a})$$

$$\hat{m}_{b \rightarrow i} = \tanh \beta J_b \prod_{j \in \partial b \setminus i} m_{j \rightarrow b}, \quad (\text{B2b})$$

where $\setminus i$ means that the weight i should be excluded from the set. $m_{i \rightarrow a}$ is interpreted as the message passing from weight i to interaction a , and $\hat{m}_{b \rightarrow i}$ is interpreted as the message passing from interaction b to weight i . By iterating these equations from some random initialization, the iteration will converge to a fixed point $\{m_{i \rightarrow a}^*\}$, which can be used to compute thermodynamic moments for learning (introduced below) and entropy (used for landscape analysis). We remark that the fixed point corresponds to a local minimum of the free energy function. The algorithm may not converge when the model becomes glassy.

We can directly compute the magnetization $m_i = \langle \sigma_i \rangle$, and correlation $C_a = \langle \sigma_i \sigma_j \rangle$ from the fixed point $\{m_{i \rightarrow a}^*\}$ as follows,

$$m_i = \tanh \left(\beta h_i + \sum_{b \in \partial i} \tanh^{-1} \left[\tanh \beta J_b \prod_{j \in \partial b \setminus i} m_{j \rightarrow b}^* \right] \right), \quad (\text{B3a})$$

$$C_a = \frac{\tanh \beta J_a + \prod_{i \in \partial a} m_{i \rightarrow a}^*}{1 + \tanh \beta J_a \prod_{i \in \partial a} m_{i \rightarrow a}^*}. \quad (\text{B3b})$$

These moments of the effective model can be used for updating the parameters of the model, approximating the model expectation terms in the Boltzmann learning rule [Eq. (5)], which are faster in our current setting than other methods, e.g., Monte-Carlo samplings.

Given the free energy, we can estimate the energy from the standard thermodynamics relation, $E = \frac{\partial(\beta F)}{\partial \beta}$, which is given by:

$$E = - \sum_i \Delta E_i + \sum_a (|\partial a| - 1) \Delta E_a, \quad (\text{B4a})$$

$$\Delta E_i = \frac{\beta h_i \sum_{x=\pm 1} x \mathcal{H}_i(x) + \sum_{x=\pm 1} \mathcal{G}_i(x)}{\sum_{x=\pm 1} \mathcal{H}_i(x)}, \quad (\text{B4b})$$

$$\Delta E_a = \beta J_a \frac{\tanh \beta J_a + \prod_{i \in \partial a} m_{i \rightarrow a}}{1 + \tanh \beta J_a \prod_{i \in \partial a} m_{i \rightarrow a}}, \quad (\text{B4c})$$

$$(\text{B4d})$$

where

$$\begin{aligned} \mathcal{G}_i(x) = & \sum_{b \in \partial i} e^{x \beta h_i} \left[\beta J_b \sinh \beta J_b (1 + x \hat{m}_{b \rightarrow i}) \right. \\ & \left. + x \beta J_b \cosh \beta J_b (1 - \tanh^2 \beta J_b) \prod_{j \in \partial b \setminus i} m_{j \rightarrow b} \right] \\ & \times \prod_{a \in \partial i \setminus b} \cosh \beta J_a (1 + x \hat{m}_{a \rightarrow i}). \end{aligned} \quad (\text{B5})$$

The entropy of the model is defined as $S = - \sum_{\boldsymbol{\sigma}} P(\boldsymbol{\sigma}) \ln P(\boldsymbol{\sigma})$, which can be also estimated from the standard thermodynamics relation $S = -\beta F + \beta E$.

In the entropy landscape analysis, we introduce a perturbed probability distribution to explore the internal structure of the network parameter space, which is given by

$$P(\boldsymbol{\sigma}) = \frac{1}{Z} \exp \left(\beta \sum_{i < j} J_{ij} \sigma_i \sigma_j + \beta \sum_i h_i \sigma_i + x \sum_i \sigma_i^* \sigma_i \right), \quad (\text{B6})$$

where β is the inverse temperature, and x is the coupling field tuning the distance between the configuration $\boldsymbol{\sigma}$ and the reference $\boldsymbol{\sigma}^*$. With the Laplace method, the free energy density f can be approximated as $f \approx \min_{\epsilon, q} f(\epsilon, q)$, which is given by $\beta f = \beta \epsilon - xq - s(\epsilon, d)$, where ϵ is the energy density (E/N), q is the overlap $\sum_i \sigma_i \sigma_i^* / N$, $s(\epsilon, d)$ is the entropy density S/N , and d is the Hamming distance per weight related to the overlap q by $d = (1 - q)/2$. At the same time, (x, q) should obey the following equations: $\partial s(\epsilon, d) / \partial d = 2x$ and $\partial s(\epsilon, d) / \partial \epsilon = \beta$, because of the Laplace method. According to the double Legendre transform, the entropy density $s(\epsilon, d)$ is given by $s(\epsilon, q) = -\beta f + \beta \epsilon - xq$. Note that, by fixing d or ϵ , one can construct isodistance or isoenergy curves just through finding compatible x or β

for the following equations:

$$\frac{\partial(\beta f)}{\partial\beta} = \epsilon, \quad (\text{B7a})$$

$$\frac{\partial(\beta f)}{\partial x} = -q, \quad (\text{B7b})$$

due to the Legendre transform.

Under the perturbed probability measure, the cavity method is still applicable, with an only change for the bias h_i as $\beta h_i \rightarrow \beta h_i + x\sigma_i^*$. By iterating the same message passing equations to a fixed point, we can finally obtain the free energy density, energy density and entropy density, etc. Note that q is computed via $\sum_i m_i \sigma_i^*/N$, where m_i is the fixed-point magnetization.

Appendix C: Simulation details

The MNIST handwritten digits dataset is a classification benchmark dataset which contains 60 000 training images and 10 000 test images. The image is a 28×28 gray-scale handwriting digit with a label taken from one of 0 to 9. For the sake of simplicity, the dataset we use for training is re-generated by applying the PCA to the original dataset. More precisely, we apply the PCA on training images to compute the eigenvectors first, and then project training and test images with these eigenvectors to finally obtain the low dimensional (20 pixels) images.

To both have a high test accuracy and avoid a large network-parameter size at the same time, we choose the network architecture as 20-15-15-10, where each number denotes the corresponding layer-width. We add a softmax layer onto the output layer and use the cross entropy as the loss function. One training epoch involves the whole training dataset, which is divided into 300 mini-batches, each of which contains 200 images. The loss is optimized by Adam [40] and the initial learning rate is set to 0.3. During the training, we also introduce an L_2 regularization to the loss function to penalize large external fields. The regularization strength is set to 10^{-5} , which is optimal for our experiments.

The stimulation details presented above apply to the case of under-parametrization. We also design two other kinds of training scenarios. The first case is the over-parametrization scenario, where the number of training images is smaller than the number of network parameters. In this case, we only train 500 images which are divided into 25 mini-batches with the mini-batch size of 20. Other hyper-parameters remain unchanged. The second case is the shallow-network scenario, where we delete all hidden layers, and thus the network architecture changes to 20-10. Other hyper-parameters remain unchanged as well. Following the same weight-collection procedure as the under-parametrization case except for setting the accuracy threshold to 70%, we collect one million and half a million weight configurations for the over-parameterization and shallow-network scenarios, respectively, in order to construct effective models.

Finally, we show additional landscape analysis when the reference weight configuration is selected from the high and medium energy regions. A qualitative same behavior is identified (Fig. 5 and Fig. 6). In addition, the histograms of model parameters inferred from the weight data are also shown in Fig. 7 for the shallow-network setting.

-
- [1] Ian Goodfellow, Yoshua Bengio, and Aaron Courville. *Deep Learning*. MIT Press, Cambridge, MA, 2016.
 - [2] Giuseppe Carleo, J. Ignacio Cirac, Kyle Cranmer, Laurent Daudet, Maria Schuld, Naftali Tishby, Leslie Vogt-Maranto, and Lenka Zdeborova. Machine learning and the physical sciences. *Reviews of Modern Physics*, 91(4):45002, 2019.
 - [3] Terrence J. Sejnowski. The unreasonable effectiveness of deep learning in artificial intelligence. *Proceedings of the National Academy of Sciences (in press)*, 2020.
 - [4] Mario Geiger, Stefano Spigler, Stephane d’Ascoli, Levent Sagun, Marco Baity-Jesi, Giulio Biroli, and Matthieu Wyart. The jamming transition as a paradigm to understand the loss landscape of deep neural networks. *Phys. Rev. E*, 100:012115, 2019.
 - [5] Quynh Nguyen and Matthias Hein. The loss surface of deep and wide neural networks. In *arXiv:1704.08045, in ICML*, 2017.
 - [6] Felix Dr axler, Kambis Veschgini, Manfred Salmhofer, and Fred A. Hamprecht. Essentially no barriers in neural network energy landscape. In *ICML*, 2018.
 - [7] Timur Garipov, Pavel Izmailov, Dmitrii Podoprikin, Dmitry Vetrov, and Andrew Wilson. Loss surfaces, mode connectivity, and fast ensembling of dnns. In *NIPS 2018: The 32nd Annual Conference on Neural Information Processing Systems*, pages 8789–8798, 2018.
 - [8] Quynh Nguyen. On connected sublevel sets in deep learning. In *ICML*, 2019.

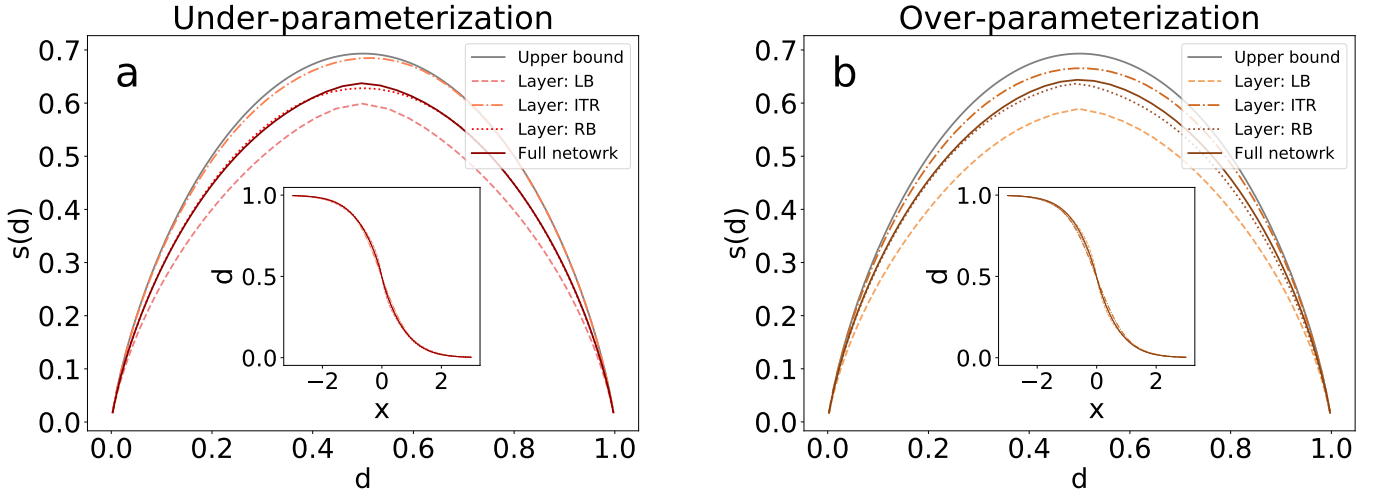


FIG. 5: Entropy landscape analyses in the high-energy references case. The reference weight configurations are randomly selected from the high-energy region, which displays no significant difference from the low-energy reference case [Fig. (4)]. (a) Under-parametrization case. (b) Over-parametrization case.

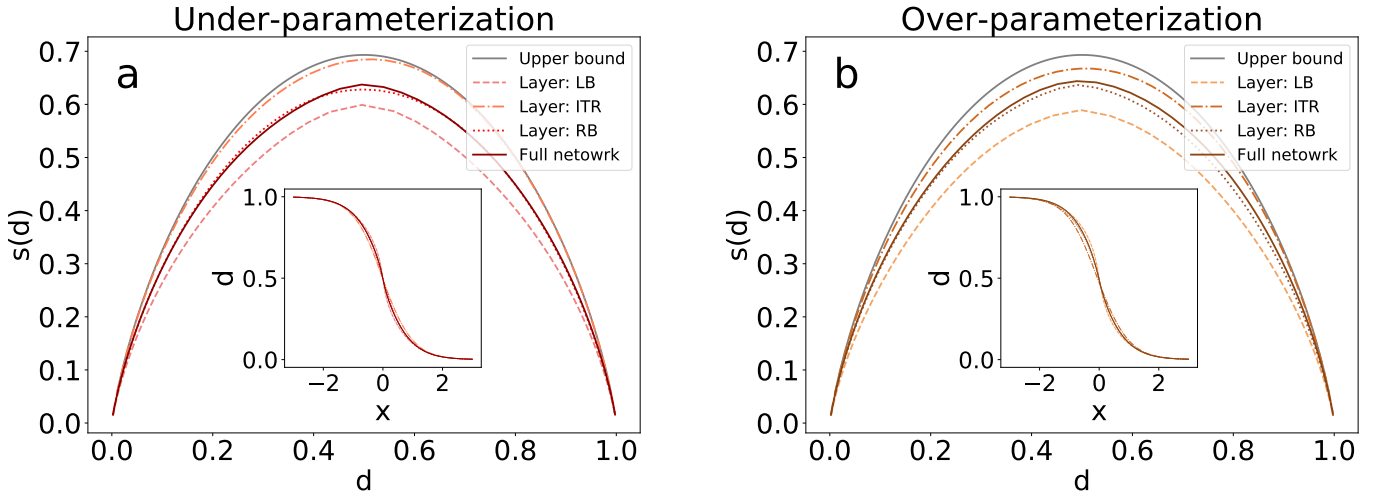


FIG. 6: Entropy landscape analyses in the medium-energy reference case. The reference weight configurations are randomly selected from the medium-energy region, which displays no significant difference from the low-energy reference case [Fig. (4)]. (a) Under-parametrization case. (b) Over-parametrization case.

- [9] Stanislav Fort and Stanislaw Jastrzebski. Large scale structure of neural network loss landscapes. In *arXiv:1906.04724*, in *NeurIPS*, 2019.
- [10] Andrew J. Ballard, Ritankar Das, Stefano Martiniani, Dhagash Mehta, Levent Sagun, Jacob D. Stevenson, and David J. Wales. Perspective: Energy landscapes for machine learning. *Physical chemistry chemical physics : PCCP*, 19:12585–12603, 2017.
- [11] Levent Sagun, Utku Evci, V. Ugur Güney, Yann Dauphin, and Léon Bottou. Empirical analysis of the hessian of over-parametrized neural networks. *arXiv:1706.04454*, 2017.
- [12] Hao Li, Zheng Xu, Gavin Taylor, and Tom Goldstein. Visualizing the loss landscape of neural nets. In *NeurIPS*, 2018.
- [13] Sepp Hochreiter and Jürgen Schmidhuber. Flat minima. *Neural Computation*, 9:1–42, 1997.
- [14] Nitish Shirish Keskar, Dheevatsa Mudigere, Jorge Nocedal, Mikhail Smelyanskiy, and Ping Tak Peter Tang. On large-batch training for deep learning: Generalization gap and sharp minima. In *arXiv:1609.04836*, in *ICLR*, 2017.
- [15] Laurent Dinh, Razvan Pascanu, Samy Bengio, and Yoshua Bengio. Sharp minima can generalize for deep nets. In *arXiv:1703.04933*, in *ICML*, 2017.
- [16] Carlo Baldassi, Fabrizio Pittorino, and Riccardo Zecchina. Shaping the learning landscape in neural networks around wide flat minima. *Proceedings of the National Academy of Sciences of the United States of America*, 117:161–170, 2019.
- [17] Pratik Chaudhari, Anna Choromanska, Stefano Soatto, Yann LeCun, Carlo Baldassi, Christian Borgs, Jennifer T. Chayes, Levent Sagun, and Riccardo Zecchina. Entropy-sgd: Biasing gradient descent into wide valleys. In *arXiv:1611.01838*, in

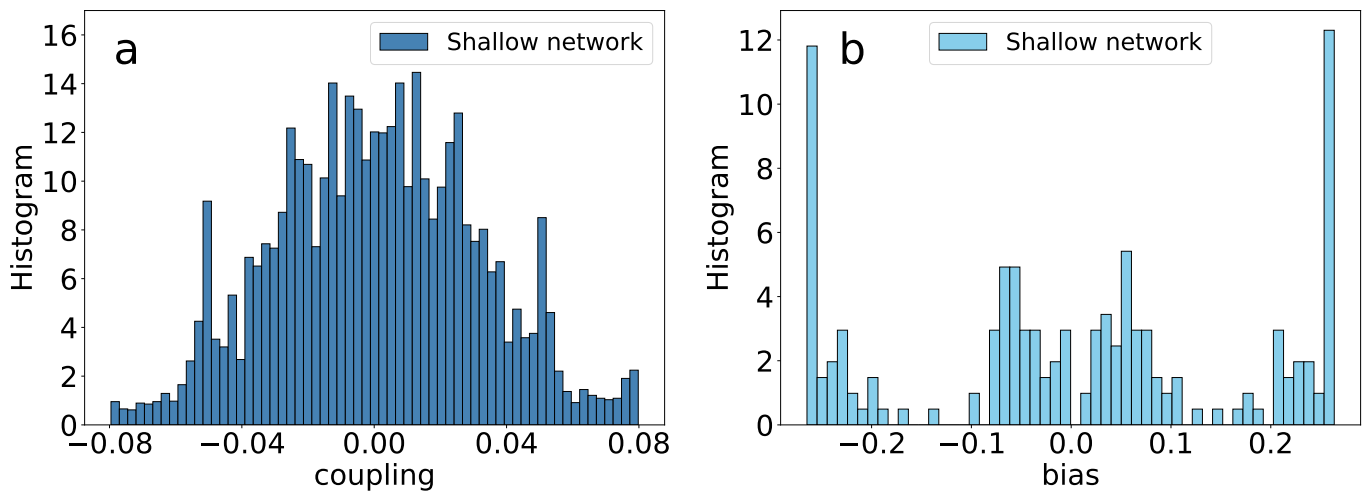


FIG. 7: Histograms of model parameters in the Ising model of the shallow-network case. (a) Histogram of inferred couplings. The couplings are distributed relatively broader compared with non-shallow networks. (b) Histogram of the inferred biases. The biases are also distributed broadly.

ICLR, 2017.

- [18] Yan V. Fyodorov and Ian Williams. Replica symmetry breaking condition exposed by random matrix calculation of landscape complexity. *Journal of Statistical Physics*, 129(5):1081–1116, 2007.
- [19] Anna Choromanska, Mikael Henaff, Michaël Mathieu, Gérard Ben Arous, and Yann LeCun. The loss surfaces of multilayer networks. In *AISTATS*, 2014.
- [20] Haiping Huang and Alireza Goudarzi. Random active path model of deep neural networks with diluted binary synapses. *Physical Review E*, 98(4):42311, 2018.
- [21] Simon Becker, Yao Zhang, and Alpha A. Lee. Geometry of energy landscapes and the optimizability of deep neural networks. *Physical review letters*, 124:108301, 2020.
- [22] Haiping Huang, K Y Michael Wong, and Yoshiyuki Kabashima. Entropy landscape of solutions in the binary perceptron problem. *J. Phys. A: Math. Theor.*, 46:375002, 2013.
- [23] Haiping Huang and Yoshiyuki Kabashima. Origin of the computational hardness for learning with binary synapses. *Physical Review E*, 90(5):52813, 2014.
- [24] Carlo Baldassi, Alessandro Ingrosso, Carlo Lucibello, Luca Saglietti, and Riccardo Zecchina. Subdominant dense clusters allow for simple learning and high computational performance in neural networks with discrete synapses. *Phys. Rev. Lett.*, 115:128101, 2015.
- [25] Oran Shayer, Dan Levi, and Ethan Fetaya. Learning discrete weights using the local reparameterization trick. In *ICLR 2018 : International Conference on Learning Representations 2018*, 2018.
- [26] E. T. Jaynes. Information theory and statistical mechanics. *Physical Review*, 106(2):620–630, 1957.
- [27] Elad Schneidman, Michael J. Berry, Ronen Segev, and William Bialek. Weak pairwise correlations imply strongly correlated network states in a neural population. *Nature*, 440(7087):1007–1012, 2006.
- [28] Haiping Huang and Taro Toyozumi. Clustering of neural code words revealed by a first-order phase transition. *Physical Review E*, 93:062416, 2016.
- [29] Hajime Yoshino. From complex to simple: hierarchical free-energy landscape renormalized in deep neural networks. *SciPost Phys. Core*, 2:5, 2020.
- [30] Chan Li and Haiping Huang. Learning credit assignment. *arXiv:2001.03354*, 2020.
- [31] Y. LeCun, The MNIST database of handwritten digits, retrieved from <http://yann.lecun.com/exdb/mnist>.
- [32] Diederik P. Kingma, Tim Salimans, and Max Welling. Variational dropout and the local reparameterization trick. In *NIPS’15 Proceedings of the 28th International Conference on Neural Information Processing Systems - Volume 2*, volume 28, pages 2575–2583, 2015.
- [33] Laurens van der Maaten and Geoffrey Hinton. Visualizing data using t-sne. *Journal of Machine Learning Research*, 9:2579–2605, 2008.
- [34] David H. Ackley, Geoffrey E. Hinton, and Terrence J. Sejnowski. A learning algorithm for boltzmann machines. *Cognitive Science*, 9(1):147–169, 1985.
- [35] Johanni Brea, Berfin Simsek, Bernd Illing, and Wulfram Gerstner. Weight-space symmetry in deep networks gives rise to permutation saddles, connected by equal-loss valleys across the loss landscape. *arXiv:1907.02911*, 2019.
- [36] S Spigler, M Geiger, S d’Ascoli, L Sagun, G Biroli, and M Wyart. A jamming transition from under- to over-parametrization affects generalization in deep learning. *Journal of Physics A: Mathematical and Theoretical*, 52:474001, 2019.
- [37] Marc Mezard and Giorgio Parisi. The bethe lattice spin glass revisited. *European Physical Journal B*, 20(2):217–233, 2001.
- [38] M. Mézard and A. Montanari. *Information, Physics, and Computation*. Oxford University Press, Oxford, 2009.

- [39] Haiping Huang. Theory of population coupling and applications to describe high order correlations in large populations of interacting neurons. *J. Stat. Mech.*, 2017(3):033501, 2017.
- [40] Diederik P. Kingma and Jimmy Lei Ba. Adam: A method for stochastic optimization. In *ICLR 2015 : International Conference on Learning Representations 2015*, 2015.